Diffusion and submonolayer growth of para-sexiphenyl on Ir(111) and Ir(111)-supported graphene

G. Hlawacek
F. S. Khokar
R. van Gastel
C. Teichert
B. Poelsema

Transparent, flexible, and conductive graphene sheets form an ideal substrate for the fabrication of organic light-emitting diodes. In order to obtain an optimal final device, it is vitally important to understand the underlying nucleation and growth processes. Here, the growth of para-sexiphenyl (6P) thin films on Ir(111)-supported graphene and on Ir(111) has been investigated. Special attention has been given to directed and concerted diffusion processes of 6P molecules on graphene grown on Ir(111). From the movement of large islands, which are formed by flat-lying molecules, across wrinkle-free graphene areas, the activation barrier for the diffusion of 6P molecules along step edges of 6P islands has been estimated to be approximately 0.26 eV. For the case of 6P growth on Ir(111), ramified islands formed by upright-standing molecules are found. Here, heteronucleation, in combination with particularities in the shape of possible smallest stable clusters, is identified as the root cause for the measured critical nucleus size of zero.

Introduction

The full understanding of growth mechanisms and molecular processes during the deposition of organic thin films is a prerequisite for the further advent of organic electronics [1]. Devices based on small conjugated molecules are starting to enter the market but are limited in performance. These limitations arise at least partially from rough film morphology, misaligned grains, and the resulting grain boundaries [2, 3]. Although the understanding of the underlying growth processes is currently improving rapidly [4, 5], a widely accepted method for achieving the desired layer-by-layer growth is still to be found. An extensive growth study of the organic semiconductor molecule para-sexiphenyl (6P) on metal-supported graphene flakes, as well as on their Ir(111) metal support, has been performed by our group [6, 7]. The achieved layer-by-layer growth at low temperatures and the transition to a Stranski-Krastanov-like growth at a relatively high temperature is rooted in the interactions of 6P with both graphene and its supporting substrate Ir(111).

Digital Object Identifier: 10.1147/JRD.2011.2160303

In this paper, we describe in detail the nucleation, island evolution, and diffusion of 6P deposited on graphene flakes and on "clean" Ir(111) parts. The substrate-induced changes of the diffusion behavior are described in detail, and models for the critical nucleus are proposed.

The combination of the organic semiconductor 6P, graphene, and the well-established deposition technique of organic molecular-beam deposition (OMBD) will allow future flexible and low-cost devices based on small conjugated molecules. 6P is well suited for the fabrication of blue [8] or color-tunable [9] light-emitting diodes. In addition, graphene is a flexible, highly conductive, and transparent electrode material [10, 11], ideally suited as a technological substrate for organic semiconductors [12, 13].

Methods

Graphene flakes were grown on an Ir(111) surface [14]. The metal crystal was cleaned by high-temperature exposure to oxygen. Graphene was then formed by thermal decomposition of ethylene on the hot Ir(111) surface [15]. Sublimation-purified 6P was purchased from TCI Europe N.V. Low-boiling-point impurities were carefully removed by thoroughly outgassing the source material for

0018-8646/11/$5.00 © 2011 IBM

several hours. 6P was deposited onto the sample by means of a resistively heated Knudsen-cell evaporator designed for organic molecules. The substrate temperature was fixed at 240 K during deposition.

An Elmitec low-energy electron microscope (LEEM) III was used to record images every second. The growth of graphene was followed in real time using photoemission electron microscopy (PEEM) until sufficiently large flakes had formed on the surface. The molecular film formation was followed using LEEM with a start voltage of 2 eV, well below the band gap of 3.1 eV for 6P. As a result, no beam-induced degradation of the films was observed.

6P on graphene flakes

The layer-by-layer growth of 6P on graphene flakes at 240 K proceeds in an interesting two-step mechanism. In the first step, islands, composed of a relatively low density of flat-lying molecules, are formed on the graphene surface. With increasing coverage, these transform into a denser full first monolayer (ML) that now exhibits the structure of the $(1\bar{1}\bar{1})$ plane of bulk 6P, i.e., the layer then consists of interdigitating rows of molecules, rotated with respect to one another. This process is described in full detail elsewhere [6]. However, the nucleation and growth of the initial islands, as well as their mobility, require more specific attention.

Figure 1 shows three LEEM images recorded within a time period of 2 seconds. Figure 1(a) shows the initial situation. An island has nucleated next to a wrinkle and has grown to a size of roughly 50,000 nm^2. The aspect ratio of the island is 1.0:1.9. Figure 1(b) shows the same island only one second later. It has elongated (aspect ratio: 1:3; size: 55,000 nm^2) and is about to detach from the wrinkle that acted as the nucleation site. When again, one second later, the process is completed [see Figure 1(c)], the center of mass of the island has moved 280 nm. The new position is clearly detached from the original nucleation site. The island shape returns to a more rounded outline (aspect ratio: 1.0:2.3; size: 61,000 nm^2) after the movement is completed. Note that deposition continued during the sequence of images.

Careful analysis of many nucleation events reveals that the 6P islands start to grow in areas close to the wrinkles or next to wrinkle crossings. Highly curved graphene areas as the wrinkles themselves are unfavorable for the deposition of organic molecules [16]. Nevertheless, the islands nucleate in close proximity of the wrinkles. This can be explained by the following observation.

The wrinkles are formed during cool down of graphene to room temperature in order to relieve compressive stress that originates from the different thermal expansion coefficients of graphene and Ir [17, 18]. This stress relief is most effective close to the wrinkles, leading to nearly strain-free graphene in those regions. In areas further away from the wrinkles, compressive strain will remain. It is well known that for metallic systems, diffusion is faster on compressively strained areas [19–21]. Assuming the same behavior for 6P on graphene leads to a higher diffusion rate further away from the wrinkles, as compared to areas adjacent to the wrinkles. A higher diffusion rate will reduce the nucleation density on the strained part of the graphene, and nucleation will preferentially occur close to the wrinkles.

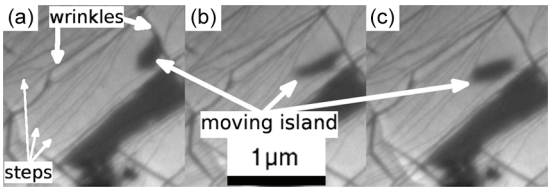

Figure 1

Three consecutive LEEM images (1 second between images) showing the mobility of the initial islands (dark patches) on graphene. A few graphene wrinkles (thick lines) and steps in the Ir(111) surface (thin lines) are marked. From left to right: A small 6P island is nucleated in the upper right corner next to a wrinkle and grows in size. When the accumulated stress reaches a critical level (middle image), the island elongates and detaches from the original site in order to move to a location further away from the wrinkle. The entire process takes 2 seconds.

The growth of the 6P island is characterized by an extremely high molecular mobility, even at low temperatures. Subsequently, at low coverage, 6P islands can arrange in a way that minimizes free energy. Although islands "prefer" to nucleate close to the wrinkles, they eventually change shape and diffuse to different locations on the graphene flake. At least two possible driving forces can be brought forward to account for this.

First, a strain-based argument is given as a possible driving force for the island movement. A delicate balance between the size and shape of a 6P island and the total strain energy it holds is one of the possible driving forces [22, 23]. As the island grows, tensile strain in the island will increase. This stress is a result of the lower density of the initial layer, as compared to the later-formed bulk structure and the mismatch between the phenyl ring spacing and the graphene ring spacing. Depending on the balance between stress and the step free energy, this can result in a shape transition of the island [24]. In our scenario, however, an additional pathway for relieving the strain exists. As mentioned, metal-supported graphene flakes are known to have areas that exhibit different levels of compressive strain. This compressive strain is lower next to wrinkles than further away from these defects. Depending on the local environment, a large island can thus become more stable in a more strained area, which is found further away from the wrinkles. On a compressively strained graphene, the molecules and the phenyl rings can relax into closer packing and, therefore, reduce the tensile strain in the island.

A second argument is based on changes in the electronic structure. The electronic structure of graphene changes under the influence of the Ir(111) surface and the strain field created by the epitaxial mismatch [25]. Therefore, different properties can be expected in areas adjacent to the wrinkles and further away from them. Little is known about the precise electronic interaction between 6P and graphene. However, a slight charge transfer from 6P to the graphene can be expected based on theoretical work done for benzene on graphene [26]. From our experiments, we have no means to differentiate between the two scenarios. Most likely, both effects are active but with different strengths.

During the transition shown in Figure 1, an area of 55,000 nm^2 has been cleared from the 6P molecules. The size of the unit cell, which contains one molecule, is 1.56 nm^2 [6]. Assuming that the motion of 6P molecules proceeds along the edges of the island, we can estimate that at least 35,000 6P molecules are needed to move from the back to the front of the island. This corresponds to a distance of 400 nm. Assuming the smallest possible step to be on the order of the graphene lattice constant (2.46 Å), a total of $\nu = 2.9 \times 10^7$ hops are necessary to complete the process. This is an upper limit of hops for a directed movement of the molecules along the rim of the island. The activation barrier E_A can then be calculated from

$$\nu = \nu_0 e^{-\frac{E_A}{kT}},$$

where ν_0 is the attempt frequency, k is the Boltzmann's constant, and $T = 240$ K for the described scenario. Using $\nu_0 = 1 \times 10^{13}$ s^{-1}, an activation energy value of $E_A = 0.26$ eV is obtained. However, for organic molecules, high attempt frequencies for desorption are reported experimentally [27–30] and theoretically [31–33]. For 6P, in particular, an extreme value of $\nu_0 = 5.6 \times 10^{25}$ s^{-1} is reported for desorption experiments [29]. Furthermore, a recent study of 6P on modified mica shows that the preexponential factor for surface diffusion is also increased by four orders of magnitude [34]. In addition, Schunack et al. have observed an anomalous amount of long jumps in the surface diffusion of large organic molecules [35]. Both effects, i.e., changes in the apparent attempt frequency and heaped occurrence of long jumps, might influence this value.

Although this activation barrier for diffusion is still a lower limit, since we assume a directed diffusion process along the edge of the island, it roughly agrees with other diffusion-related values known for 6P. The binding energy of benzene on graphene has been calculated to be on the order of 0.16–0.24 eV [26]. As a first-order approximation, 6P can be seen as a linear combination of six benzene rings. The binding energy of 6P on graphene is therefore expected to be between 1 and 1.46 eV. The values for the diffusion energy values reported here, despite sizable uncertainties, are substantially lower and thus do not conflict with the estimated binding energy.

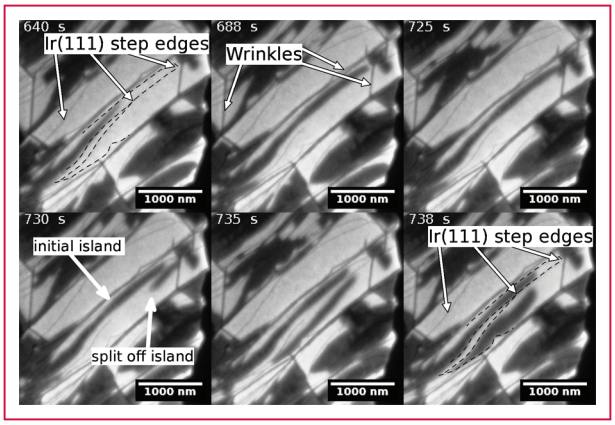

Figure 2

Sequence of LEEM images recorded during the deposition of 6P on graphene at 240 K. A narrow island (dark patches in the center), which is confined between two steps, slowly grows and finally fills the area enclosed by the steps (deposition time from 640 to 688 seconds). Thirty-two seconds later, the island overcomes the step and spills out onto the adjacent graphene-covered Ir(111) terrace (725 seconds of deposition). As the island on the new terrace grows in size (730 seconds of deposition), it moves away from the low-strain area next to a wrinkle (735 seconds of 6P deposition). After reaching an area where the strain mismatch between the big 6P island and graphene is reduced, it starts to fill the entire area by reducing its aspect ratio (738 seconds of deposition). Please be aware of the nonuniform time step between the images. Wrinkles and Ir(111) step edges are marked by arrows and dashed lines to guide the eye.

Processes, as illustrated in Figure 1, are always observed to be confined in an area enclosed by wrinkles. Often, the path of the islands is also confined by steps in the underlying Ir. The increased curvature of the graphene sheet at the position of the Ir(111) step poses a small but observable obstacle to the growth of the 6P islands. However, the effect is smaller than that due to the wrinkles. **Figure 2** depicts an island that is first overcoming a step edge, then splits in two, and finally moves across the graphene flake. Initially, the island grows in size without crossing the surrounding steps until 720 seconds of 6P deposition. It then suddenly crosses the small end of the step-enclosed area and spills out on the next graphene-covered terrace. There, it quickly grows in size, covering the area next to the wrinkle. As in the aforementioned situation, when a certain size is reached, it detaches from the wrinkle (island size: 117,400 nm^2; aspect ratio: 1:10) and, for this particular case, also separates from the initial island. It continues to grow (final island size: 300,000 nm^2; maximum aspect ratio: 1:13) while the center of mass moves 810 nm across the surface. After reaching an area where the mismatch between the 6P island and the strained graphene becomes small enough, the shape

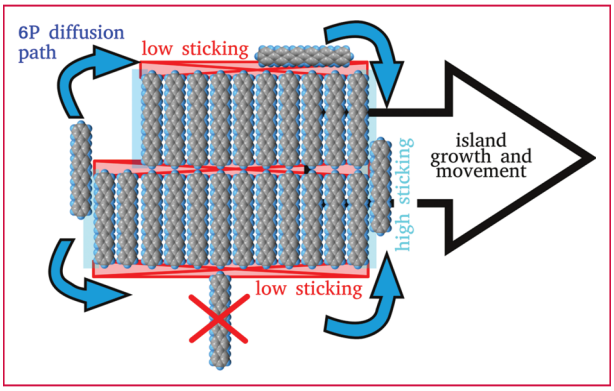

Figure 3

Schematic 6P islands outlining the possible diffusion paths and preferred incorporation sites. 6P molecules detach from the left and move toward the right side of the island. The side facets are formed by the terminating hydrogen atoms of 6P and possess a low sticking probability. Only the facets terminated by the long side of 6P have a high sticking probability due to the large number of hydrogen bonds that can be formed there.

transition is also reversed, leading again to a lower aspect ratio of 1:6.

A detailed micro-low-energy electron diffraction (μ-LEED) study reveals the precise orientation of the molecules with respect to graphene lattice [6]. However, a relation of these data to the real-space orientation of the molecules in each island is difficult, if not impossible, to determine. From the way that the islands move on the surface, we can directly deduct the molecular orientation of the island in real space. **Figure 3** schematically shows a 6P island on a surface. Molecules are detaching from the left-hand side and diffusing to the right-hand side of the island (these are the edges parallel to the molecular axis, referred to as the *parallel edges*). This could be caused by a strain field induced by a wrinkle on the left side and the island exceeding a certain size. As the molecule diffuses around the island, no stable bond can be formed at the edge perpendicular to the long molecular axis (referred to as the *perpendicular edge*). Either the crystalline symmetry of the island has to be broken or the molecule is connected only by a single hydrogen bond. Both situations are unfavorable compared to incorporation at the parallel edge, where at least six hydrogen bonds can be formed without breaking the symmetry of the crystalline structure. This is a well-known behavior of many anisotropic molecules. For thicker films, it will lead to the frequently observed needle- or chain-like growth of 3-D islands [36, 37]. In these 3-D structures, the molecular axis is oriented perpendicular to the fiber axis. For flat-lying 6P molecules on graphene, it leads to an anisotropic growth and directed movement of the islands. The preferred direction of island growth and movement is perpendicular to the long molecular axis of the 6P molecules forming the island.

The frequency at which these processes occur and the speed of the actual transformation result from the high diffusion rate of individual 6P molecules in this configuration. As soon as any interdigitating edge-on molecules are added to complete the first ML, the mobility of islands is reduced to a negligible value on the timescale of our experiment. For higher layers, no island mobility is observed. Compared with the first half layer, they constitute a more stable structure. This is also evident when comparing the open structure of the initial layer to the more bulk-like arrangement of the thicker films [6].

6P on Ir(111)

Figure 4(a) shows a graphene-free part of the iridium surface after the deposition of 6P has been stopped. A relatively large number of small irregularly shaped islands are visible. From μ-LEED measurements, we obtain a typical intermolecular distance of 4.4 Å. This corresponds to the distance between the center molecule and the corner molecules in the (100)-plane of bulk 6P. The irregularly shaped islands on the Ir(111) surface are therefore formed from upright- standing 6P molecules. Converting the coverage measured on the graphene flakes of 4.35 ML [6] of flat-lying molecules to upright-standing molecules, one expects 0.8 ML of upright-standing 6P. The coverage obtained from analyzing the LEEM images is only 0.5 ML. However, it is well known that a high step-edge barrier, which is effective during the growth of upright 6P islands, leads to a pronounced mound formation [4]. Assuming Poisson-shaped mounds, the expected first layer coverage is 55% for a nominal film thickness of 0.8 ML and this is in good agreement with the measured value.

In comparison to Figures 1 and 2, it is evident that the nucleation density $N_s = 7.2\ \mu m^{-2}$ on the iridium surface is substantially higher than that for graphene, although no numbers can be given for the latter surface. From the capture-zone distribution, we can calculate the size of the critical nucleus, using the distribution function of the general Wigner-Seitz surmise, as proposed in [38]:

$$P_\beta(s) = a_\beta s^\beta e^{-b_\beta s^2}.$$

Here, a_β and b_β are constants given by the normalization and unit-mean conditions, respectively.[1] The fluctuating variable $s = A/\langle A\rangle$ is obtained from the areas of the Voronoi cells around the center of mass for each island. The only fit parameter $\beta = i + 2$ [39] allows the direct extraction of the critical nucleus size. In **Figure 4(b)**, the capture-zone distribution for 6P islands on Ir(111) at 240 K is shown. The best fit ($\beta = 1.6$) and the curves for $\beta = 1$, 2, and 3 are

[1] $a_\beta = 2\Gamma((\beta+2)/2)^{\beta+1}/\Gamma((\beta+1)/2)^{\beta+2}$, and $b_\beta = [\Gamma((\beta+2)/2)/\Gamma((\beta+1)/2)]^2$. Here, the Γ symbol refers to the gamma function in mathematics.

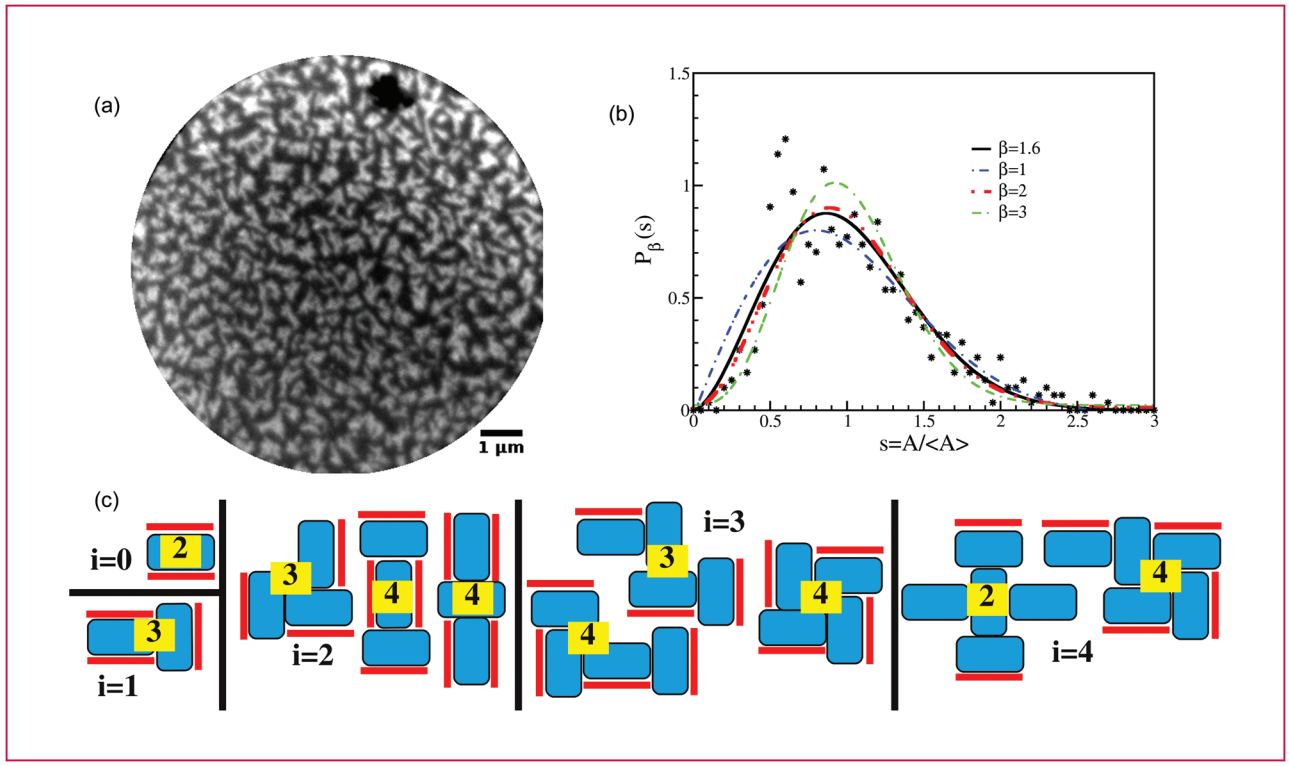

Figure 4

6P growth on Ir(111). (a) LEEM image showing small islands formed by upright-standing 6P molecules on Ir(111). Field of view = 10 μm. (b) Capture-zone distribution for 6P on Ir(111) grown at 240 K. The best fit (solid line) to the data (stars) and distribution functions of the GWS for $\beta = 1$, 2, and 3 (line styles: dash-dot, dash-dot-dot, and dash-dash-dot) are shown. (c) Possible configurations of the critical nucleus for $i = 0$ to $i = 4$. Upright-standing 6P molecules are represented by rectangles with an aspect ratio based on the Van der Waals dimensions of 6P. The π-system of the molecule is situated on the long sides of the rectangle. The central numbers on yellow background indicate the number of completely uncovered π-systems, which are marked by red bars.

shown. The critical nucleus size obtained this way is zero, which means that a single molecule would be immobile on the surface, and spontaneous nucleation proportional to the ad-molecule density should be observable.

To understand this result, we have to remember that these calculations are, strictly speaking, only valid for homogeneous nucleation. A critical nucleus size of zero can be understood in the context of heterogeneous or defect nucleation [40, 41]. Haas et al. explained the transition from $i = 0$ to $i = 3$ that they observed in the Pd/MgO system by referring to the presence of defects, which act as traps and geometrical considerations that will make $i = 3$ exceptionally stable [42]. The situation observed here is similar since both effects play a role in the growth of 6P on the Ir(111) surface.

First, it is easy to understand that the Ir(111) surface is not clean. Carbon residues, perhaps in the form of small graphene flakes, will be present all over the surface. This is also suggested by the fact that we observe upright-standing molecules. One would expect a clean metal surface to have flat-lying 6P molecules [43, 44]. However, it has been shown that small amounts of carbon on the metal surface will change the orientation of the molecules and lead to films formed by upright-standing molecules [45, 46]. Furthermore, it has been shown that defects such as dangling bonds can force molecules into an upright orientation, although they would, in principle, energetically "prefer" to lie flat on the surface [47].

Second, certain assumptions can be made about the form of the critical nucleus. It is reasonable to assume that the molecules forming the nucleus are arranged in a configuration that is close to the bulk herringbone structure. **Figure 4(c)** schematically shows 6P clusters starting from $i = 0$ to $i = 4$. The number of completely exposed π-systems is given for each configuration. It turns out that only $i = 0$ and $i = 4$ have a minimum number of two π-systems completely exposed. In general, one can assume that clusters with a small number of exposed π-systems are energetically favored. These numbers are also in reasonable good agreement with recent DFT calculations, which reveal the

smallest stable cluster size of four for upright-standing molecules [34]. As a result, for a sufficiently high trap binding energy, the formation of homogeneous nuclei with $i = 1$ to $i = 3$ is suppressed. Only at sufficiently high temperatures, small clusters trapped at an impurity will break up, and homogeneous nucleation with $i = 4$ should become effective.

Conclusion

In this paper, we have described the diffusion process of 6P molecules on graphene flakes and on iridium. The initial island formation on graphene is characterized by a high mobility value of 6P molecules. This allows for strain-driven shape and position changes of the initial sub-ML islands. A delicate interplay between intrinsic strain in the graphene flakes and strain that builds up with increasing island size is one of the possible driving forces. However, electronic effects based on charge transfer between 6P and graphene and graphene and iridium are another possible cause.

The growth of 6P on the Ir(111) surface yields ramified islands formed by upright-standing molecules. Using capture-zone scaling, we obtain a critical nucleus size of $i = 0$. This result is interpreted as an indication for heterogeneous nucleation triggered by a high density of defects. The defects are most likely carbon clusters remaining from the graphene formation or possibly small graphene flakes. As long as the trap binding energy of the defects for 6P is sufficiently high, a homogeneous nucleation with cluster size between two and three is suppressed. In addition, we have presented possible configurations for the critical nucleus for $i = 0$ to $i = 4$. Only the last one has a comparatively small number of fully exposed π-systems. We interpret this in terms of a reduced stability for the intermediate nuclei.

In a scenario where nucleation is mostly defect driven, these cluster sizes are most likely suppressed because of dominant trapping at defect sites.

References

1. C. K. Chiang, C. R. Fincher, Y. W. Park, A. J. Heeger, H. Shirakawa, E. J. Louis, S. C. Gau, and A. G. MacDiarmid, "Electrical conductivity in doped polyacetylene," *Phys. Rev. Lett.*, vol. 39, no. 17, pp. 1098–1101, Oct. 1977.
2. S. Verlaak, C. Rolin, and P. Heremans, "Microscopic description of elementary growth processes and classification of structural defects in pentacene thin films," *J. Phys. Chem. B*, vol. 111, no. 1, pp. 139–150, Jan. 2007.
3. G. Horowitz and M. E. Hajlaoui, "Mobility in polycrystalline oligothiophene field-effect transistors dependent on grain size," *Adv. Mater.*, vol. 12, no. 14, pp. 1046–1050, Jul. 2000.
4. G. Hlawacek, P. Puschnig, P. Frank, A. Winkler, C. Ambrosch-Draxl, and C. Teichert, "Characterization of step-edge barriers in organic thin-film growth," *Science*, vol. 321, no. 5885, pp. 108–111, Jul. 2008.
5. X. Zhang, E. Barrena, D. Goswami, D. G. De Oteyza, C. Weis, and H. Dosch, "Evidence for layer-dependent Ehrlich–Schwöbel barrier in organic thin film growth," *Phys. Rev. Lett.*, vol. 103, no. 13, p. 136101, Sep. 2009.
6. G. Hlawacek, F. S. Khokhar, R. van Gastel, B. Poelsema, and C. Teichert, "Smooth growth of organic semiconductor films on graphene for high-efficiency electronics," *Nano Lett.*, vol. 11, no. 2, pp. 333–337, Feb. 2011.
7. F. S. Khokar, G. Hlawacek, R. van Gastel, C. Teichert, and B. Poelsema, "The influence of substrate temperature on growth of para-sexiphenyl thin films on lr(111) supported graphene studied by LEEM," arXiv:1107.0373 [cond-mat.mtrl-sci], 2011.
8. H. Yanagi and S. Okamoto, "Orientation-controlled organic electroluminescence of p-sexiphenyl films," *Appl. Phys. Lett.*, vol. 71, no. 18, pp. 2563–2565, Nov. 1997.
9. S. Tasch, C. Brandstaetter, F. Meghdadi, G. Leising, G. Froyer, and L. Athouel, "Red-green-blue light emission from a thin film electroluminescence device based on parahexaphenyl," *Adv. Mater.*, vol. 9, no. 1, pp. 33–36, Jan. 1997.
10. A. K. Geim and K. S. Novoselov, "The rise of graphene," *Nat. Mater.*, vol. 6, no. 3, pp. 183–191, Mar. 2007.
11. T. J. Echtermeyer, M. C. Lemme, M. Baus, B. N. Szafranek, A. K. Geim, and H. Kurz, "Nonvolatile switching in graphene field-effect devices," *IEEE Electron Device Lett.*, vol. 29, no. 8, pp. 952–954, Aug. 2008.
12. P. Lauffer, K. V. Emtsev, R. Graupner, T. Seyller, and L. Ley, "Molecular and electronic structure of PTCDA on bilayer graphene on SiC(0001) studied with scanning tunneling microscopy," *Phys. Stat. Sol. (B)*, vol. 245, no. 10, pp. 2064–2067, Oct. 2008.
13. Q. H. Wang and M. C. Hersam, "Room-temperature molecular-resolution characterization of self-assembled organic monolayers on epitaxial graphene," *Nat. Chem.*, vol. 1, no. 3, pp. 206–211, Jun. 2009.
14. J. Coraux, A. T. N'Diaye, C. Busse, and T. Michely, "Structural coherency of graphene on Ir(111)," *Nano Lett.*, vol. 8, no. 2, pp. 565–570, Feb. 2008.
15. R. van Gastel, A. T. N'Diaye, D. Wall, J. Coraux, C. Busse, N. M. Buckanie, F.-J. Meyer zu Heringdorf, M. Horn von Hoegen, T. Michely, and B. Poelsema, "Selecting a single orientation for millimeter sized graphene sheets," *Appl. Phys. Lett.*, vol. 95, no. 12, pp. 121901-1–121901-3, Sep. 2009.
16. F. Tournus and J.-C. Charlier, "Ab initio study of benzene adsorption on carbon nanotubes," *Phys. Rev. B, Condens. Matter*, vol. 71, no. 16, article no. 165421, Apr. 2005.
17. A. T. N'Diaye, J. Coraux, T. N. Plasa, C. Busse, and T. Michely, "Structure of graphene on Ir(111)," *New J. Phys.*, vol. 10, article no. 043033, 2008.
18. A. T. N'Diaye, R. van Gastel, A. J. Martinez-Galera, J. Coraux, H. Hattab, D. Wall, F. Meyer zu Heringdorf, M. Horn von Hoegen, J. M. Gomez-Rodriguez, B. Poelsema, C. Busse, and T. Michely, "In situ observation of stress relaxation in epitaxial graphene," *New J. Phys.*, vol. 11, article no. 113056, 2009.
19. H. Brune, K. Bromann, H. Röder, K. Kern, J. Jacobsen, P. Stoltze, K. Jacobsen, and J. Norskov, "Effect of strain on surface diffusion and nucleation," *Phys. Rev. B, Condens. Matter*, vol. 52, no. 20, pp. R14380–R14383, Nov. 1995.
20. M. Schroeder and D. E. Wolf, "Diffusion on strained surfaces," *Surf. Sci.*, vol. 375, no. 1, pp. 129–140, Mar. 1997.
21. M. Gsell, P. Jakob, and D. Menzel, "Effect of substrate strain on adsorption," *Science*, vol. 280, no. 5364, pp. 717–720, May 1998.
22. J. Tersoff and R. M. Tromp, "Shape transition in growth of strained islands: Spontaneous formation of quantum wires," *Phys. Rev. Lett.*, vol. 70, no. 18, pp. 2782–2785, May 1993.
23. V. S. Stepanyuk, D. I. Bazhanov, W. Hergert, and J. Kirschner, "Strain and adatom motion on mesoscopic islands," *Phys. Rev. B, Condens. Matter*, vol. 63, no. 15, pp. 153406-1–153406-3, Apr. 2001.
24. H. J. W. Zandvliet and R. Van Gastel, "Bistability in the shape transition of strained islands," *Phys. Rev. Lett.*, vol. 99, no. 13, article no. 136103, Sep. 2007.
25. I. Pletikosi, M. Kralj, P. Pervan, R. Brako, J. Coraux, A. T. N'Diaye, C. Busse, and T. Michely, "Weakly interacting graphene on a metal: Dirac cones and mini gaps for C/Ir(111)," *Phys. Rev. Lett.*, vol. 102, no. 5, article no. 056808, Feb. 2009.

26. Y.-H. Zhang, K.-G. Zhou, K.-F. Xie, J. Zeng, H.-L. Zhang, and Y. Peng, "Tuning the electronic structure and transport properties of graphene by noncovalent functionalization: Effects of organic donor, acceptor and metal atoms," *Nanotechnology*, vol. 21, no. 6, article no. 065201, Feb. 2010.
27. S. L. Tait, Z. Dohnalek, C. T. Campbell, and B. D. Kay, "n-alkanes on MgO(100): II. Chain length-dependence of kinetic desorption parameters for small n-alkanes," *J. Chem. Phys.*, vol. 122, no. 16, article no. 164708, Apr. 2005.
28. P. Frank, T. Djuric, M. Koini, I. Salzmann, R. Rieger, K. Müllen, R. Resel, N. Koch, and A. Winkler, "Layer growth, thermal stability, and desorption behavior of hexaaza-triphenylene-hexacarbonitrile on Ag(111)," *J. Phys. Chem. C*, vol. 114, no. 14, pp. 6650–6657, Apr. 2010.
29. S. Müllegger and A. Winkler, "Hexaphenyl thin films on clean and carbon covered Au(111) studied with TDS and LEED," *Surf. Sci.*, vol. 600, no. 6, pp. 1290–1299, Mar. 2006.
30. K. R. Paserba and A. J. Gellman, "Kinetics and energetics of oligomer desorption from surfaces," *Phys. Rev. Lett.*, vol. 86, no. 19, pp. 4338–4341, May 2001.
31. K. A. Fichthorn, K. E. Becker, and R. A. Miron, "Molecular simulation of temperature programmed desorption," *Catal. Today*, vol. 123, no. 1–4, pp. 71–76, May 2007.
32. K. E. Becker and K. A. Fichthorn, "Accelerated molecular dynamics simulation of the thermal desorption of *n*-alkanes from the basal plane of graphite," *J. Chem. Phys.*, vol. 125, no. 18, article no. 184706, Nov. 2006.
33. K. A. Fichthorn and R. A. Miron, "Thermal desorption of large molecules from solid surfaces," *Phys. Rev. Lett.*, vol. 89, no. 19, article no. 196103, Nov. 2002.
34. T. Potocar, S. Lorbek, D. Nabok, Q. Shen, L. Tumbek, G. Hlawacek, P. Puschnig, C. Ambrosch-Draxl, C. Teichert, and A. Winkler, "Initial stages of a *para*-hexaphenyl film growth on amorphous mica," *Phys. Rev. B, Condens. Matter*, vol. 83, no. 7, pp. 075423-1–075423-10, Feb. 2011.
35. M. Schunack, T. R. Linderoth, F. Rosei, E. Laegsgaard, I. Stensgaard, and F. Besenbacher, "Long jumps in the surface diffusion of large molecules," *Phys. Rev. Lett.*, vol. 88, no. 15, article no. 156102, Apr. 2002.
36. H. Plank, R. Resel, H. Sitter, A. Andreev, N. S. Sariciftci, G. Hlawacek, C. Teichert, A. Thierry, and B. Lotz, "Molecular alignments in sexiphenyl thin films epitaxially grown on muscovite," *Thin Solid Films*, vol. 443, no. 1/2, pp. 108–114, Oct. 2003.
37. F. Balzer, V. G. Bordo, A. C. Simonsen, and H.-G. Rubahn, "Optical waveguiding in individual nanometer-scale organic fibers," *Phys. Rev. B, Condens. Matter*, vol. 67, no. 11, article no. 115408, Mar. 2003.
38. A. Pimpinelli and T. L. Einstein, "Capture-zone scaling in island nucleation: Universal fluctuation behavior," *Phys. Rev. Lett.*, vol. 99, no. 22, p. 226102, Nov. 2007.
39. A. Pimpinelli and T. L. Einstein, "Pimpinelli and Einstein reply," *Phys. Rev. Lett.*, vol. 104, no. 14, article no. 149602, Apr. 2010.
40. G. Rosenfeld, R. Servaty, C. Teichert, B. Poelsema, and G. Comsa, "Layer-by-layer growth of Ag on Ag(111) induced by enhanced nucleation: A model study for surfactant-mediated growth," *Phys. Rev. Lett.*, vol. 71, no. 6, pp. 895–898, Aug. 1993.
41. D. D. Chambliss and K. E. Johnson, "Nucleation with a critical cluster size of zero: Submonolayer Fe inclusions in Cu(100)," *Phys. Rev. B, Condens. Matter*, vol. 50, no. 7, pp. 5012–5015, Aug. 1994.
42. G. Haas, A. Menck, H. Brune, J. V. Barth, J. A. Venables, and K. Kern, "Nucleation and growth of supported clusters at defect sites: Pd/MgO(001)," *Phys. Rev. B, Condens. Matter*, vol. 61, no. 16, pp. 11 105–11 108, Apr. 2000.
43. H. Oji, E. Ito, M. Furuta, K. Kajikawa, H. Ishii, Y. Ouchi, and K. Seki, "*p*-sexiphenyl/metal interfaces studies by photoemission and metastable atom electron spectroscopy," *J. Electron Spectrosc. Relat. Phenom.*, vol. 101-103, pp. 517–521, Jun. 1999.
44. B. Winter, J. Ivanco, F. P. Netzer, and M. G. Ramsey, "Ordered mono- and multilayer films of sexiphenyl on Al(111): A LEED investigation," *Thin Solid Films*, vol. 433, no. 1/2, pp. 269–273, Jun. 2003.
45. S. Müllegger and A. Winkler, "The influence of carbon on the adsorption/desorption kinetics and monolayer formation of *p*-quaterphenyl on Au(111)," *Surf. Sci.*, vol. 574, no. 2/3, pp. 322–330, Jan. 2005.
46. P. Frank, G. Hlawacek, O. Lengyel, A. Satka, C. Teichert, R. Resel, and A. Winkler, "Influence of surface temperature and surface modifications on the initial layer growth of para-hexaphenyl on mica," *Surf. Sci.*, vol. 601, no. 10, pp. 2152–2160, May 2007.
47. L. Tsertseris and S. T. Pantelides, "Atomic scale mechanisms of selective adsorption and dimerization of pentacene on Si surfaces," *Appl. Phys. Lett.*, vol. 87, no. 23, article no. 233109, Dec. 2005.

Received December 2, 2010; accepted for publication February 11, 2011

Gregor Hlawacek *Physics of Interfaces and Nanomaterials, MESA+ Institute for Nanotechnology, University of Twente, 7500 AE Enschede, The Netherlands (g.hlawacek@tnw.utwente.nl).*

Fawad S. Khokar *Physics of Interfaces and Nanomaterials, MESA+ Institute for Nanotechnology, University of Twente, 7500 AE Enschede, The Netherlands (F.S.Khokhar@tnw.utwente.nl).*

Raoul van Gastel *Physics of Interfaces and Nanomaterials, MESA+ Institute for Nanotechnology, University of Twente, 7500 AE Enschede, The Netherlands (R.vanGastel@tnw.utwente.nl).*

Christian Teichert *Institute of Physics, University of Leoben, 8700 Leoben, Austria (teichert@unileoben.ac.at).*

Bene Poelsema *Physics of Interfaces and Nanomaterials, MESA+ Institute for Nanotechnology, University of Twente, 7500 AE Enschede, The Netherlands (b.poelsema@tnw.utwente.nl).*